International Journal of Applied Earth Observation and Geoinformation 56 (2017) 24–35

Contents lists available at ScienceDirect

International Journal of Applied Earth Observation and Geoinformation

journal homepage: www.elsevier.com/locate/jag

Assessing the influence of return density on estimation of lidar-based aboveground biomass in tropical peat swamp forests of Kalimantan, Indonesia

Solichin Manuri [a,*], Hans-Erik Andersen [b,*], Robert J. McGaughey [b], Cris Brack [a]

[a] Fenner School of Environment and Society, The Australian National University, Linnaeus way Building 141, 2601 ACT, Australia
[b] USDA Forest Service, Pacific Northwest Research Station, University of Washington, PO Box 352100, Seattle, WA, USA

ARTICLE INFO

Article history:
Received 19 July 2016
Received in revised form 21 October 2016
Accepted 1 November 2016

Keywords:
Airborne lidar
Aboveground biomass
Return proportion metric
Digital terrain model
Model regression
Model-based inference

ABSTRACT

The airborne lidar system (ALS) provides a means to efficiently monitor the status of remote tropical forests and continues to be the subject of intense evaluation. However, the cost of ALS acquisition can vary significantly depending on the acquisition parameters, particularly the return density (i.e., spatial resolution) of the lidar point cloud. This study assessed the effect of lidar return density on the accuracy of lidar metrics and regression models for estimating aboveground biomass (AGB) and basal area (BA) in tropical peat swamp forests (PSF) in Kalimantan, Indonesia. A large dataset of ALS covering an area of 123,000 ha was used in this study. This study found that cumulative return proportion (CRP) variables represent a better accumulation of AGB over tree heights than height-related variables. The CRP variables in power models explained 80.9% and 90.9% of the BA and AGB variations, respectively. Further, it was found that low-density (and low-cost) lidar should be considered as a feasible option for assessing AGB and BA in vast areas of flat, lowland PSF. The performance of the models generated using reduced return densities as low as 1/9 returns per m^2 also yielded strong agreement with the original high-density data. The use model-based statistical inferences enabled relatively precise estimates of the mean AGB at the landscape scale to be obtained with a fairly low-density of 1/4 returns per m^2, with less than 10% standard error (SE). Further, even when very low-density lidar data was used (i.e., 1/49 returns per m^2) the bias of the mean AGB estimates were still less than 10% with a SE of approximately 15%. This study also investigated the influence of different DTM resolutions for normalizing the elevation during the generation of forest-related lidar metrics using various return densities point cloud. We found that the high-resolution digital terrain model (DTM) had little effect on the accuracy of lidar metrics calculation in PSF. The accuracy of low-density lidar metrics in PSF was more influenced by the density of aboveground returns, rather than the last return. This is due to the flat topography of the study area. The results of this study will be valuable for future economical and feasible assessments of forest metrics over large areas of tropical peat swamp ecosystems.

1. Introduction

Peat swamp forests (PSF) have been recognised as important forest ecosystems due to their large capacity for terrestrial carbon storage (Page et al., 2011). However, an enormous amount of carbon is emitted when PSF are cleared, degraded or converted to agricultural land (Miettinen et al., 2012). High emissions also result from peat decomposition (Hergoualc'h and Verchot, 2014; Hooijer et al., 2006) and peat land fires (Page et al., 2002). Page et al. (2002) estimated that approximately 0.9 gigatons of carbon was emitted from peat fires in 1997. The figure was far greater than Indonesia's annual emissions from deforestation and forest degradation from 2000 to 2012 (MoEF, 2015). In recent decades, PSF in South East Asia have contributed the largest portion of global greenhouse gas (GHG) emissions from the land use, land use change and forestry (LULUCF) sector (Murdiyarso et al., 2010). The majority of such emissions come from peat soil oxidation due to fires; however, the loss of aboveground primary vegetation plays a crucial role in increasing the likelihood of the occurrence of fires (Siegert et al., 2001). Despite their critical role in climate change mitigation,

* Corresponding authors.
E-mail addresses: solichin.solichin@anu.edu.au, solichin.manuri@gmail.com (S. Manuri), handersen@fs.fed.us (H.-E. Andersen).

http://dx.doi.org/10.1016/j.jag.2016.11.002
0303-2434/

estimates of emission factors from PSF in Indonesia remain scarce and are far from accurate (MoEF, 2015).

Due to a combination of factors, including limited studies at the landscape scale, reliance on low-resolution remotely-sensed data and the absence of locally-developed tree biomass models, global-scale aboveground biomass (AGB) estimates for tropical forests have generally had high levels of uncertainty (Houghton et al., 2012). A review of previous studies showed high levels of variability in the AGB estimates within Indonesian PSF mainly due to limited sample sizes (MoEF, 2015). Establishing plots within PSF of Indonesia is logistically difficult and labour intensive; thus, field studies are expensive and spatially limited. Consequently, there has been strong interest in the use of remote sensing to decrease the costs and increase the efficiency of forest assessments and monitoring in Indonesian PSF.

Tools such as radar and high-resolution optical satellite imagery have been used to support forest inventory in PSF; however, the results of previous studies, particularly, in terms of predictive power, were not favourable (Englhart et al., 2011; Hirata et al., 2014; Schlund et al., 2015). For example, the coefficients of determination (R^2) (a statistical measure of the strength of the regression relationship between remote sensing metrics and AGB measurements) have been found to range from 0.5 to 0.65. Conversely, studies using airborne lidar system (ALS) yielded significantly more precise estimates of AGB in PSF with R^2 values of lidar derived metrics and AGB that range from 0.77 to 0.88 (Englhart et al., 2013; Jubanski et al., 2012).

However, compared to satellite-based remote sensing technologies, the costs associated with ALS acquisitions are relatively high; for example, at a small scale, the overall cost of ALS can approach that of ground measurements for a forest stand assessment (Hummel et al., 2011). Given that the largest component of the costs of a lidar acquisition is aeroplane flight time, it is more economical to acquire lidar by having an aircraft fly higher and faster; however, all other things being equal, this results in a lidar point cloud that has a lower return density (and thus poorer spatial resolution). Flying at a higher altitude not only affects reduced return density and intensity, but also increases footprint size. Footprint size may affect the accuracy of individual tree measurements (Andersen et al., 2006); however, it has an insignificant effect on area-based forest metrics assessments (Goodwin et al., 2006; Næsset, 2004).

Studies assessing the effect of return density on the accuracy of lidar derived forest metrics have mostly been conducted in temperate and boreal regions (Gobakken and Næsset, 2008; Jakubowski et al., 2013; Magnusson et al., 2007; Singh et al., 2015; Watt et al., 2014), but have been limited to tropical regions (Hansen et al., 2015). In mountainous regions, the use of low-density lidar should be avoided due to potentially large errors in the terrain model that can have deleterious effects on the accuracy of canopy height metrics (Leitold et al., 2015). However, it should be noted that other studies conducted in areas of complex topography have shown that highly accurate inventory estimates can be obtained using relatively low return densities (i.e., 1–2 returns per m^2 for biomass (Jakubowski et al., 2013) and 2–3 returns per m^2 for timber volume (Watt et al., 2014). Further, Ruiz et al. (2014) found that reducing return density to 1/4 returns per m^2 continued to provide good estimates of AGB in a steep terrain, suggesting that the size of field plots was crucial to the development of lidar metric models.

The majority of previous lidar studies have used direct canopy height metrics (Drake et al., 2003; Jubanski et al., 2012) and canopy height-related statistical metrics (d'Oliveira et al., 2012; Singh et al., 2015) to develop predictive models for forest inventory parameters. Such models have been shown to be more accurate in less-diverse temperate forests (Lefsky et al., 2005) than tropical forest regions (Andersen et al., 2014; Asner and Mascaro, 2014). A number of recent studies have explored the use of return proportion-related parameters (Ioki et al., 2014; Sheridan et al., 2014) and developed multivariate models that include the return proportion at 20–25 m height as an independent variable; however, the performance of these models was no better than that obtained using mean aboveground height parameters (Ioki et al., 2014). This type of model could be suitable for areas dominated by less disturbed forests, but is not suitable for areas characterised by a wide range of degraded conditions and succession levels.

The overall objective of this study was to demonstrate the ability of ALS in AGB estimation and mapping in large area of degraded tropical PSF in Central Kalimantan, Indonesia. The specific objectives of the study were to: identify the best AGB and basal area (BA) models using canopy height-related and return proportion parameters at various return density levels; assess the sensitivity of lidar metrics associated with reduced return densities; and estimate AGB levels for a large peat swamp area, using a model-based estimation/inferential framework. It appears that this study was the first to assess the effect of lidar return density on the estimation of AGB in tropical PSF.

2. Materials and methods

2.1. Study site

The study site was the former Kalimantan Forest Carbon Partnership (KFCP) project area, located in the Ex-Mega Rice Project (EMRP) in peat land of Central Kalimantan Indonesia (114° 23.5′–114° 40.3′ E; 1° 56.0′ to 2° 30.1′ S) (see Fig. 1). The KFCP boundary encompasses 123,608 ha of tropical PSF with a range of degradation levels. The topography of the area is very flat with elevations of 1–20 m above sea level and slope less than 0.1%. Peat dome fringes have their lowest elevations near riverbanks, but these elevations slowly increase as they approach the center of the dome.

From 2003 to 2010, the mean annual rainfall was 2900 mm (Ichsan et al., 2013) and the dry seasons (in which the monthly rainfall was less than 200 mm) were from June to September. From the 1970s to the 1990s, large concessionaires selectively logged the forest and small scale illegal logging continues today. Forests with a high variation of succession and high degradation levels dominated the northern part of the study site. The forests were dominated by non-dipterocarp species, including *Combretocarpus rotundatus, Campnosperma coriaceum, Tetractomia obovatum* and *Palaquium cochleariifolium.* The dominant tree species from dipterocarp family included *Shorea teysmaniana* and *Shorea balangeran*. Conversely, as a result of logging, land clearing and frequent fires, the southern part of the study site was covered by shrubs, ferns or grasslands (Graham et al., 2014) (see Fig. 2).

The tropical PSFs in Borneo occur in peat soil which developed from the accumulation of dead vegetation in a waterlogged environment since more than 30,000 years ago (Page et al., 2004). PSFs are considered to be the highest carbon stock ecosystem but lower in biodiversity and productivity, than the neighbouring lowland dipterocarp forests. The soil nutrient deficiency and acidity are increased toward the center of the dome, where the peat is deeper, providing a limiting factors for vegetation to grow. Thus, only low pole trees could grow in the peat dome center, commonly dominated by *Combretocarpus* sp and *Dacrydum* sp (Morley, 1981). In contrast, primary PSFs grow in the fringe of the dome harbour large emergent and commercial trees such as *Shorea spp* from dipterocarp family, *Agathis sp*, *Koompassia sp*, *Palaquium sp* and *Gonystylus bancanus* with maximum tree height between 40 and 45 m (Anderson, 1963; Page et al., 1999) (see Fig. 2).

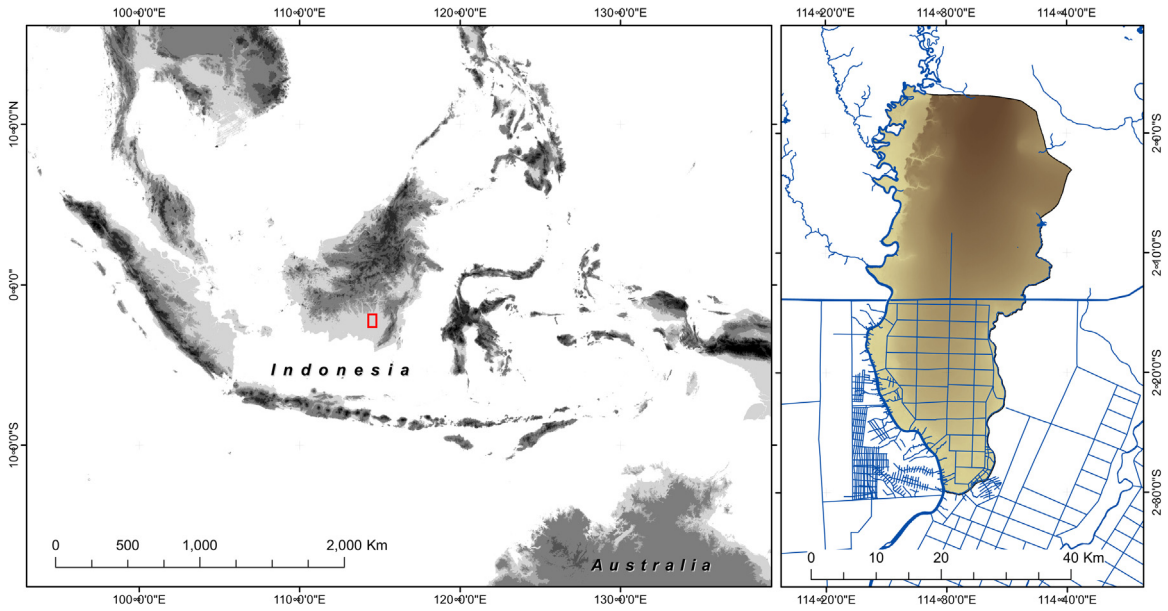

Fig. 1. Maps of the study area. KFCP boundary is depicted on the right map. Darker greyscales represent higher elevation.

Fig. 2. (a) Primary succession of tropical PSF, showing a multi layered canopy with some emergent tall trees; (b) logged over PSF with a newly excavated canal for transportation, managed under large timber concession; (c) small-scale logging operation is typically under management of local community or in many cases it was often considered as illegal logging; (d) heavily degraded PSF due to unsustainable logging and recurrent fires, dominated by ferns.

2.2. Ground measurements

The KFCP project established permanent plots for vegetation monitoring that were systematically placed in eight randomly selected zones representing land cover classes and disturbance levels (Graham et al., 2014). Five zones were located near large canals and in highly degraded areas, while the other three zones were located in closed-canopy forests. Within each zone, three transects, spaced 150 m apart, were placed perpendicular to the canals or in an east to west direction from randomly located starting points.

Table 1
Specifications for lidar data acquisition at KFCP (Ballhorn et al., 2014).

Variable	Value
Laser pulse frequency (KHz)	100
Scan frequency	45
Half scan angle (°)	22
Flying height (m)	800
Speed (knots)	110
Side overlap (%)	30
Net swath width (m)	450
Calculated return density (return per m^2)	2.8

Four plots were established on each transect at a distance of 50, 100, 400 and 700 m from the canals or the starting points. The scientific names of the species, the diameters at breast height (DBH) or above buttress and the height of all the trees within the plot were recorded. Square nested-plots of 1 m × 1 m, 8 m × 8 m, 16 m × 16 m and 32 m × 32 m were established for seedlings (less than 1.5 m in height), saplings (with a height greater 1.5 m and DBH less than 10 cm), poles (with a DBH greater than 10 cm but less than 20 cm) and trees (with a DBH greater than 20 cm), respectively. A total of 88 plots were measured in mid-2011 and at the beginning of 2012. The other eight plots were measured in 2013, two years after lidar acquisition, and thus excluded from the analysis.

2.3. Lidar data sets

Lidar data sets were provided by the KFCP project. Lidar data of KFCP areas were captured with an intended density of 2 returns per m^2. Due to a 30% overlapping swath area, the calculated return density was 2.8 returns per m^2. All datasets were captured using Optech ALTM 3100 and Optech Orion M200 instruments mounted on a Pilatus Porter fixed wing aircraft (Table 1). The same vendor collected data from 15 August to 2 October 2011. The vendor provided a 1 m resolution lidar derived digital terrain model (DTM) for the KFCP area. The vendor also classified ground and non-ground points. The vertical accuracy of the raw lidar data and the DTM products were 0.14 m and 0.18 m, respectively (Ballhorn et al., 2014).

2.4. Field plot data analysis

AGB and BA were calculated for 88 and 72 plots, respectively. There were fewer plots for the BA because there were no saplings or trees in 16 plots. Mixed species AGB equations for PSFs were used to estimate AGB for trees with DBH greater than 2 cm. Two multi-parameter AGB equations were selected. The first used DBH, wood density (WD) and height (see Eq. (1)) and the second used DBH and height (see Eq. (2)) (Manuri et al., 2014).

$$AGB = 0.15D^{2.095}WD^{0.664}H^{0.552} \quad (1)$$

$$AGB = 0.081D^{2.049}H^{0.672} \quad (2)$$

Where AGB is in Kg, D is DBH or above buttress in centimetres, WD is in gr.cm^{-3} and H is tree height in metres. The models were developed from relatively large sample size (n = 148), more than the minimum sample size suggested by Roxburgh et al. (2015) for developing generic allometric models. The samples were collected using destructive sampling in PSF in Sumatra and West Kalimantan, covering a wide range of tree size, with maximum tree diameter and height of 176 cm and 49.5 m, respectively. These models predicted tree AGB better than other local models in a PSF in Central Kalimantan through a validation using destructive sampling data (Manuri et al., 2015).

To calculate AGB, WD values for each species were derived from the WD global database (Zanne et al., 2009) using values associated with related tree species names or genus names. WD values were not assigned for unidentified tree species. Eq. (2) was used to estimate the AGB of unidentified trees. The average AGB for seedlings less than 1.5 m in height were estimated as 0.10 kg, as there was no destructive sampling data from seedlings and undergrowth. AGB and BA were calculated in Mg ha^{-1} and m^2 ha^{-1}, respectively and summarised to the plot level.

2.5. Lidar processing

Data processing flows and the associated specific objectives were presented in Fig. 3. FUSION v3.42 was used to process all point cloud lidar data (McGaughey, 2014). To compute products over the entire acquisition area, the Lidar Toolkit (LTK) Processor tool was used in FUSION to create and manage the processing workflow.

The lidar return densities were reduced from the original density to simulate different acquisition specifications for the lidar data. We used ThinData utility in FUSION to reduce the lidar returns from 2.8 returns per m^2 to 1 return per 100 m^2. The points were selected randomly in cell sizes of 25 m^2. The return density of lidar data was reduced from 2.8 to 2, 1, 1/4, 1/9, 1/16, 1/25, 1/36, 1/49, 1/64, 1/81, 1/100 returns per m^2 that were equivalent to a return spacing of 1/2, 1–10 m, respectively. A similar approach has been applied in other studies (Leitold et al., 2015; Magnusson et al., 2007; Ruiz et al., 2014; Strunk et al., 2012).

Ground points were filtered using the GroundFilter utility with a grid size of 16 m. Two scenarios were applied to assess the effect of point density on the regression models. In the first scenario, each thinned dataset was normalised using the original DTM delivered by the lidar provider to remove terrain influence on vegetation height. In the second scenario, the thinned dataset was normalised using the corresponding DTM created from the thinned point data. In relation to all return densities, a 1 m resolution of DTM was created using the TINSurface utility. This utility created a triangular irregular network (TIN) surface and then interpolated a regular grid at the desired resolution.

Using the original and thinned point cloud data, lidar metrics were computed for each plot area so that they could be used as predictor variables in the regression models. Ground points and low vegetation (less than 1 m) returns were excluded from the metric computation. Several lidar metrics were calculated in relation to vegetation heights (i.e. mean aboveground height (MAH), quadratic mean aboveground height (QMAH), variance of aboveground height (VAR) and height percentiles (P)) and return proportions (i.e. density of return points (RD), cumulative return proportion (CRP), quadratic cumulative return proportion (QCRP), return proportion of certain height stratum (Str) and cumulative return proportion of height strata (CStr)) (see Table 2). Several authors have used different terminologies to describe return proportion, including laser penetration (Ioki et al., 2014) and point frequency or density (Sheridan et al., 2014). This paper defined return density as the total number of returns per area and return proportion as the ratio of the number of returns above a certain height and the total number of returns (Table 2 and Fig. 4).

2.6. Regression analysis of aboveground biomass models

Regression modelling of field-measured AGB data was used to evaluate lidar metrics at the plot level and determine the best-fitting AGB (Mg ha^{-1}) and BA (m^2 ha^{-1}) models. All metrics (including aboveground height-related metrics, height percentiles and return proportions) that had previously been reported to be correlated with AGB were tested for significance using ordinary least square (OLS) regression. Models with insignificant variables (i.e., p-values larger than 0.05) were excluded. Collinearity in the multivariate regression models was evaluated using the variance inflation factor (VIF). Models with VIFs greater than five were

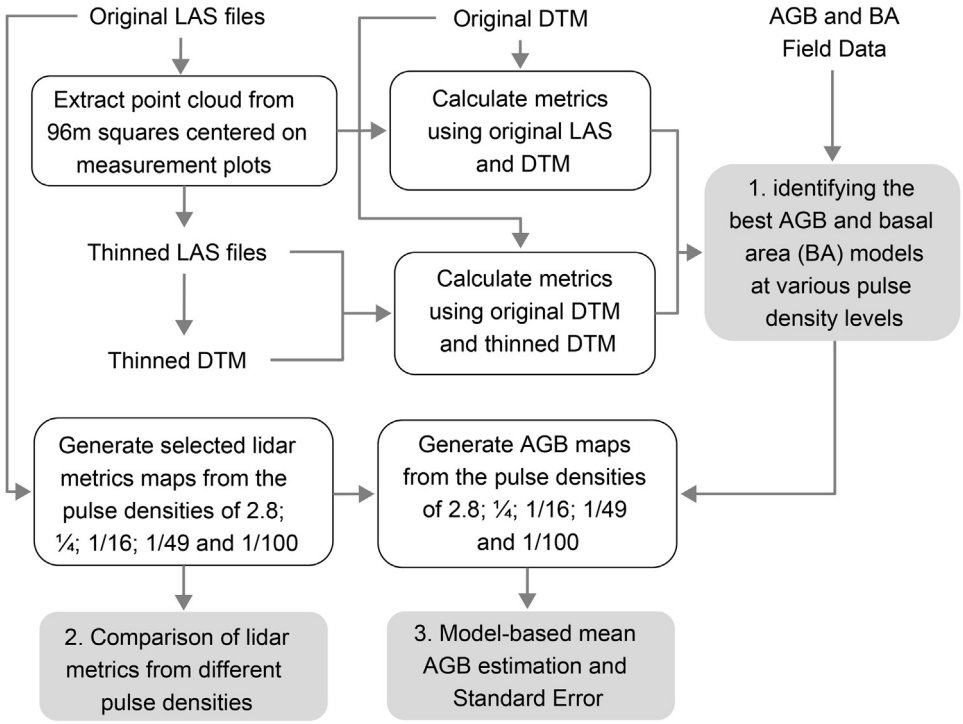

Fig. 3. Flowchart of lidar analysis in this study. The grey boxes represent the specific objectives.

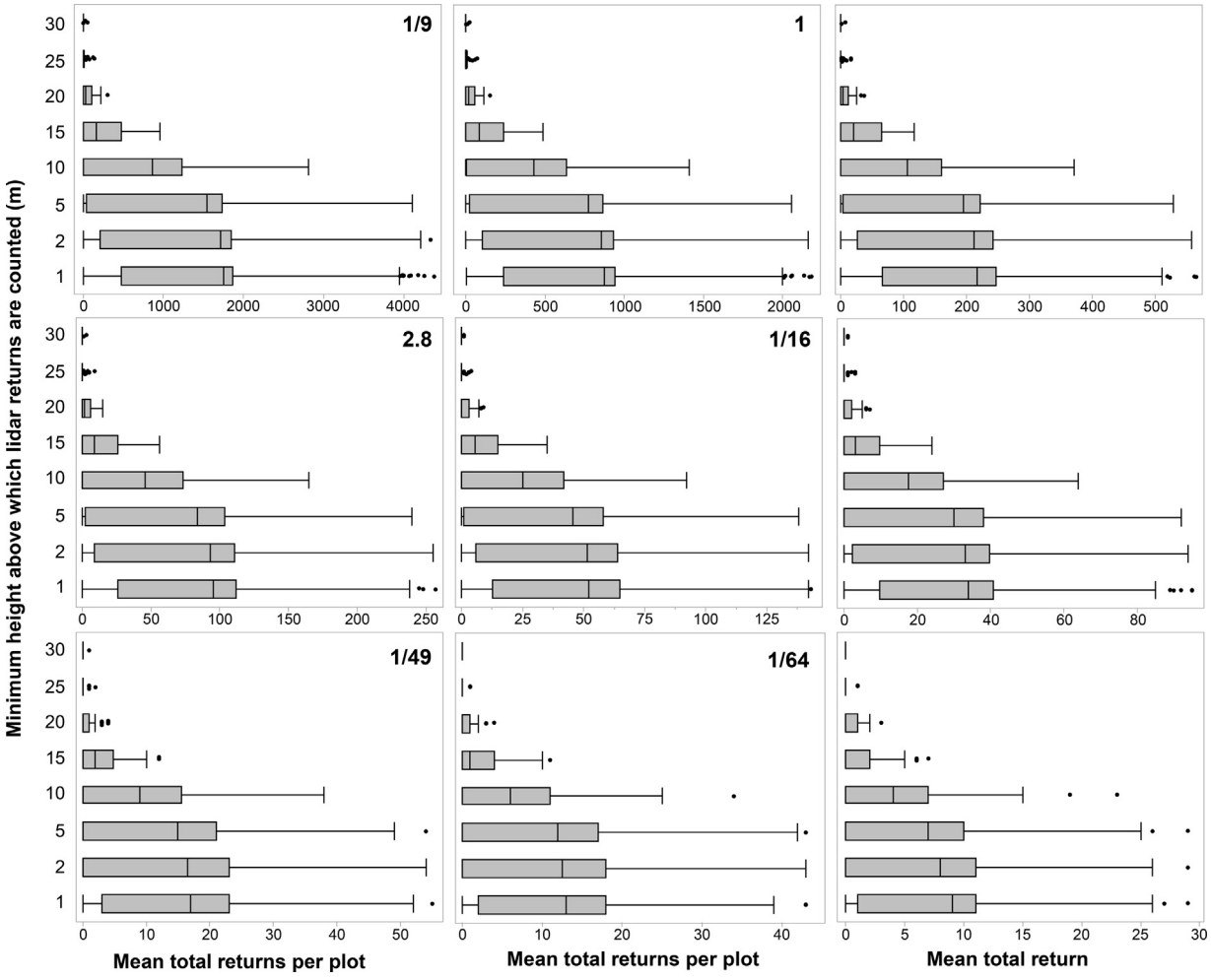

Fig. 4. Boxplot of mean total returns per plot (32 m × 32 m) above various height at different thinning levels.

Table 2
Summary of the lidar forest structure variables derived from the lidar point cloud for each ground plot used in this study.

Metric symbol	Description
MAH	Mean height of aboveground canopy
QMAH	Quadratic value of MAH = $(MAH)^2$
VAH	Height variance of aboveground canopy
P1, P5, P10, P20, P25, P 30, P40, P50, P60, P70, P75, P80, P90, P95, P99	Percentile height values of the aboveground returns
RD1, RD5, RD10, RD15, RD20, RD25 and RD30	Density of return points above 1, 5, 10, 15, 20, 25 and 30 m heights, derived by dividing total number of returns above specific height with area size
RP1, RP5, RP10, RP15, RP20, RP25 and RP30	Return proportion above 1, 5, 10, 15, 20, 25 and 30 m heights, are the ratio of return number above specific height and total number of returns
CRP	Cumulative return proportions is the sum of all RP values
QCRP	Quadratic cumulative return proportions is the quadratic value of CRP = $(CRP)^2$
Str1-5; Str5-10; Str10-15; Str15-20; Str20-25 and Str25-30	Return proportion of canopy height strata (Str) is the ratio of return number at specific height strata/bin and total number of returns
CStr	Cumulative number of return proportion of canopy height strata (Str)

excluded (Sileshi, 2014). The relationship between AGB and lidar metrics was modelled using simple and multivariate linear model forms. When residuals of a linear model did not depict a normal distribution, the variable was then fitted using a non-linear model form. The linear models were fitted using OLS regression, while the power models were fitted using non-linear regression. The best and the most parsimonious models were selected based on the significant parameter estimates, highest R^2 and the lowest root mean square errors (RMSE) while still having a normal distribution of residuals. We validated the models using 10-fold cross validation technique (Kohavi, 1995). We used JMP 11 software (SAS, 2015) for the regression modelling and R statistical package (R-Development-Core, 2013) for 10-fold cross validation and full coverage AGB estimation using variance estimator.

2.7. Comparing lidar metrics to assess the effect of return density

Lidar derived metrics generated from four different return densities (i.e. 1/4, 1/16, 1/49 and 1/100) were compared with the original lidar metric. Different terrain models were also generated for each density level. A total of 1192 sampling points were selected across the KFCP area using a systematic grid of sample points spaced 1 km apart. All lidar metrics for the sample locations were extracted from raster layers covering the entire acquisition area. Scatter plots were produced for each metric and compared. The R^2, RMSE, intercept and slope deviation of the fitted line between lidar metrics were generated using the reduced density data and original high return data. An intercept of 0 and a slope of 1 indicated unbiased.

2.8. AGB estimates using variance estimator

To assess the influence of lidar return density on the precision of mean biomass estimates, a model-based approach was used to estimate the mean biomass and the variance of this estimate for different thinning levels (2.8, 1/4, 1/16, 1/49 and 1/100 returns per m^2) covering whole study site. We generated lidar metrics for different thinning levels with 30-m resolution. As stated above, the KFCP site was approximately 123,608 ha and thus resulting in 1,330,748 30-m pixels. Adopting the approach of (McRoberts, 2010), if Y represents the random variable of AGB with a mean μ and standard deviation σ, the observed AGB at the i^{th} pixel (y_i) was represented as: $y_i = \mu_i + \varepsilon_i$ where $\varepsilon_i \sim N\left(0, \sigma^2\right)$. The mean AGB at the i^{th} pixel was then given by $\mu_i = f\left(\boldsymbol{X_i}; \boldsymbol{\beta}\right)$ (as estimated by $\hat{\mu}_i = f\left(\boldsymbol{X_i}; \hat{\boldsymbol{\beta}}\right)$). Where $\boldsymbol{X_i}$ is the lidar-based predictor variable at the i^{th} pixel and $\hat{\boldsymbol{\beta}}$ is the vector of p predicted regression coefficients (p = 2, in this case). The model-based estimate of mean AGB over the entire areas was $\frac{1}{N}\sum_{i=1}^{N}\hat{\mu}_i$. The variance of the model-based mean AGB estimate was given by:

$$\hat{V}\left[\frac{1}{N}\sum_{i=1}^{N}\hat{\mu}_i\right] = \frac{1}{N^2}\sum_{i=1}^{N}\sum_{j=1}^{N}\hat{Cov}(\hat{\mu}_i, \hat{\mu}_j) = \frac{1}{N^2}\sum_{i=1}^{N}\sum_{i=1}^{N}\boldsymbol{Z_{i_i}'}\boldsymbol{V}_{\hat{\beta}}\boldsymbol{Z_j} \quad (3)$$

Where $\boldsymbol{V}_{\hat{\beta}}$ is the variance-covariance matrix for the regression model parameter estimates. For the case of p = 2 (and for this study), $\boldsymbol{V}_{\hat{\beta}}$ was given by:

$$\begin{bmatrix} \hat{V}\left(\hat{\beta}_0\right) & \hat{Cov}\left(\hat{\beta}_0, \hat{\beta}_1\right) \\ \hat{Cov}\left(\hat{\beta}_1, \hat{\beta}_0\right) & \hat{V}\left(\hat{\beta}_1\right) \end{bmatrix} \quad (4)$$

Where the elements of $\boldsymbol{Z}$ was given by:

$$z_j = \frac{\partial\left(\boldsymbol{X}; \hat{\boldsymbol{\beta}}\right)}{\partial\beta_j} \quad (5)$$

As shown by the above variance formula, the calculation of an exact variance would entail a computationally difficult double summation over a total of N × N pixels (1,330,748 × 1,330,748 = 1.7 trillion pixels). (McRoberts, 2010) demonstrated that the variance could be closely approximated by using a sample of the pixels in which sampled pixels were on an equally-spaced, two-dimensional, perpendicular grid over the entire area:

$$\hat{V}\left[\frac{1}{N}\sum_{i=1}^{N}\hat{\mu}_i\right] \approx \frac{1}{{n_{grid}}^2}\sum_{i=1}^{n_{grid}}\sum_{j=1}^{n_{grid}}\boldsymbol{Z_{i_i}'}\boldsymbol{V}_{\hat{\beta}}\boldsymbol{Z_j} \quad (6)$$

Further, McRoberts et al. (2013) showed that any detrimental effects of using the gridded sample to calculate the variance estimate were negligible for grid widths (i.e., spacing) up to $n_p = 100$ population units (pixels).

3. Results

3.1. Regressions models for BA and AGB estimation

The 10 best models were selected for BA and AGB estimation from linear, multivariate linear and non-linear regressions based on their residual distribution, R^2 and RMSE. The selected BA and AGB models had R^2 of more than 0.70 and 0.85, respectively (see Tables 3 and 4). All return density and height percentiles metrics failed to fulfil good model requirements due to insignificant parameters, low R^2, high RMSE and non-normal residual distribution. The best percentile parameters for the models were $a + b \times P40$ and $a + b \times P25 + c \times VAR$ (see Models No. 1 and 8 in Tables 3 and 4).

Other linear models also had similar trends in their residual distributions (i.e., the $a + b \times MAH$ and $a + b \times CRP$). Similar to Sheridan

Table 3
Parameter estimates of BA models using full density data (2.8 returns per m^2). Significance is indicated by *** for $p < 0.001$; ** for $p < 0.01$; * for $p < 0.05$ and ns for not significant.

Model No	BA Model	Parameter estimates				R^2	RMSE
		a	b	c	d		
1	a+b × P40	−5.722*	4.065***			0.754	7.04
2	a+b × MAH	−9.591**	3.983***			0.729	7.37
3	a+b × CRP	−6.856**	12.541***			0.777	6.70
4	a+b × QMAH	4.312ns	0.238***			0.701	7.75
5	a+b × QCRP	2.373ns	2.870***			0.809	6.19
6	a+b × CStr	5.326ns	57.028***			0.780	6.65
7	a+b × Str15+c × Str20+d × Str25	5.281**	60.145***	57.992***	32.978ns	0.790	6.60
8	a+b × P25 + c × Var	−3.532	4.691***	0.1.5ns		0.752	7.11
9	a × MAH^b	1.090	1.433			0.753	7.43
10	a × CRP^b	15.516	2.212			0.809	6.20

Table 4
Parameter estimates of AGB models using full density data (2.8 returns per m^2). Significance is indicated by *** for $p < 0.001$; ** for $p < 0.01$; * for $p < 0.05$ and ns for not significant.

Model No	AGB Model	Parameter estimates				R^2	RMSE
		a	b	c	d		
1	a+b × P40	−46.351***	27.639***			0.891	38.3
2	a+b × MAH	−67.710***	26.484***			0.857	44.0
3	a+b × CRP	−29.625**	77.251***			0.858	43.9
4	a+b × QMAH	−5.174ns	1.831***			0.883	39.8
5	a+b × QCRP	−1.405 ns	20.328***			0.907	35.5
6	a+b × CStr	7.640 ns	425.756***			0.890	38.6
7	a+b × Str10+c × Str15+d × Str20	10.590 ns	371.400***	529.170***	502.928*	0.898	37.5
8	a+b × P25 + c × Var	−43.230***	32.161***	0.546ns		0.882	40.3
9	a × MAH^b	1.938	1.968			0.884	39.7
10	a × CRP^b	15.516	2.212			0.909	35.2

et al. (2014), this study also confirmed the heteroscedasticity of the residuals using these parameters. These models were thus excluded in the next step of the analysis.

The power models using CRP variable explained 80.9% and 90.9% of the BA and AGB variations, respectively. These fits were similar or slightly better than those of squared CRP (QCRP) linear models. However, the regressions between predicted and observed values from all linear models had better-fitted lines than power models with slopes not significantly different from 1 and intercepts not significantly different from 0. A 10-fold cross-validation confirmed the lowest RMSE for all CRP-related models (Fig 5.).

Most of the return proportion models demonstrated normal residual plots except the linear CRP model. The models' errors were distributed near zero. However, all models tended to have low precision in estimating small AGB. This may be attributable to the exclusion of AGB measurement from shrubs or grasses in the plots. The majority of the highly degraded peat swamps were dominated by lower vegetation such as grasses, shrubs, sedges or ferns (Rieley and Ahmad-Shah, 1996). Only tree species were recorded on the plots. Thus, the biomass values of highly degraded PSF did not completely represent the actual biomass in the plots. These models also tended to under-estimate lower biomass and over-estimate large biomass (see Fig 5). There are two potential reason for this trend: first, similar to Magnusson et al. (2007), we found in these large AGB plots, understorey vegetation are abundant (small trees occupying second layer canopy). The other reason could be due to the model form. Similar trend was found by Englhart et al. (2013) when applying power model. They further suggested to use 2 equations: i.e. power model for low AGB and linear for high AGB values.

3.2. Influence of return density on model performance

Overall, the R^2 of BA and AGB models, where the point clouds were normalised using the original high-resolution DTM, declined by 12–30% as return density decreased to 0.01 or 1/100 returns per m^2 (see Fig. 6). The R^2 and RMSE of the models remained stable until 1/9 returns per m^2. Below this point, the performance of the models decreased slightly until 1/49 density. Then, they either remained stable or declined further. The decreases of R^2 were comparable to a previous study by (Singh et al., 2015) of an urban forest in a relatively flat area.

As expected, the performance of the models that had been built with data in which the elevations were normalised using the thinned DTM data, declined more drastically than the performance of the models, which normalised using the high-resolution DTM, especially the models with return density lower than 1/9 returns per m^2 (see Fig. 6A2 and B2). The difference in R^2 varied from 25 to 60%. The R^2 of the lowest density power CRP model that used high-resolution DTM, declined by only 12% from the model with the highest return density. The performance of these models was similar between 2 and 1/9 returns per m^2.

The CRP power models performed similarly to the QCRP linear models until 1/9 returns per m^2 in estimating the AGB (see Fig. 6). Below this density, the CRP power model outperformed the QCRP linear models. Most of the BA and AGB models with reduced DTM depicted unstable declines except the linear model of CStr. The performance of the CStr model was similar to the CRP power model and QCRP linear model in estimating BA until density declined to 1/4 returns per m^2. After which, the performance of the model decreased sharply to its lowest level.

3.3. Return density effects on lidar metrics

The lidar derived metrics of four different return densities (i.e., 1/4 1/16, 1/49 and 1/100) were compared with the original lidar metric. Three lidar metrics were considered in the comparative analysis (i.e., maximum height (H max)), QMAH and QCRP). All of the lidar metrics derived from the 1/4 return density data had a high correlation with the metrics derived from the original, higher-density data with a R^2 of more than 0.96 and slopes very close to 1. Further reductions in return density produced a poorer correlation with the original data and led to an underestimation of the metrics.

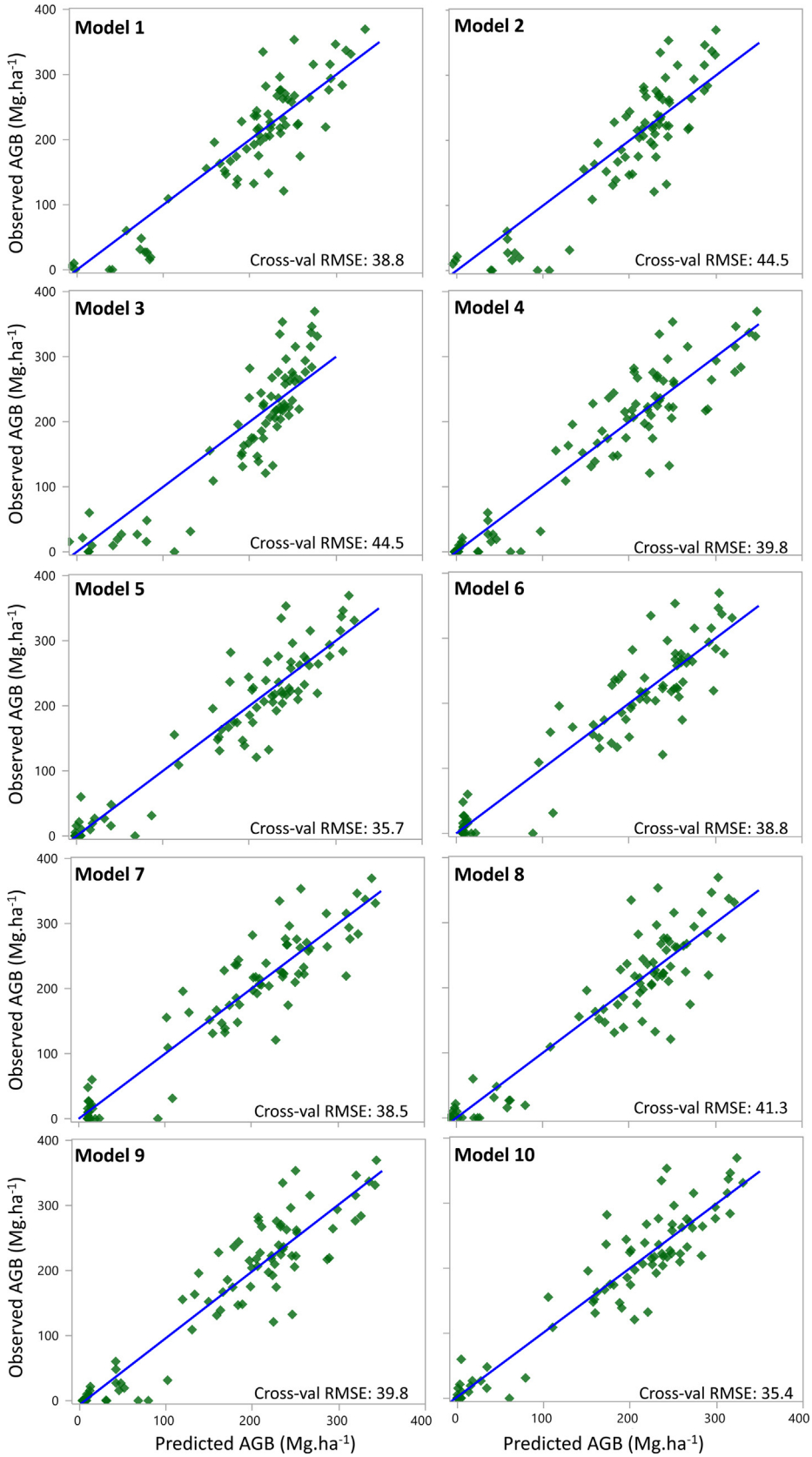

Fig. 5. Scatterplot of observed against predicted AGB per plot from the best models as shown in Table 4. Cross-val RMSE is the root mean square error from 10-fold cross validation.

Table 5
QCRP linear regression models and their variance-covariance for different lidar densities.

Lidar density	Parameter estimates		R^2	Variance Intercept	Variance QCRP	Covariance
	a	b				
2.8	−1.405	20.328	0.91	45.59	0.49	−3.92
1/4	7.52	36.3	0.91	42.55	1.58	−6.67
1/16	15.29	37.229	0.86	60.89	2.59	−10.12
1/49	6.487	37.114	0.82	83.95	3.37	−13.86
1/100	70.96	25.372	0.48	178.40	8.42	−28.47

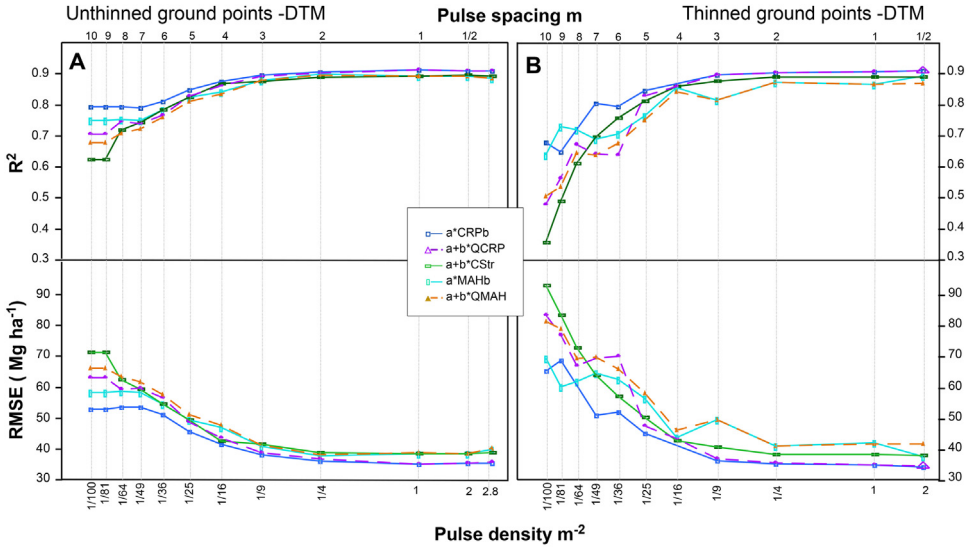

Fig. 6. AGB (A) and BA (B) models performance at various return densities.

The DTM effects on the reduced density lidar metrics were also assessed. Specifically, the metrics that had been normalised using the original high-resolution DTM were compared with the metrics that had been normalised using the thinned DTM data. The lidar metrics calculated using the thinned DTM had a similar correlation to the ones calculated using high-resolution DTM (see Fig 7). However, reducing the return density had the greatest effect on the H max metric compared to the other metrics. An underestimation of the H max was clearly observed in low return density metrics as indicated by larger intercepts of the fitted lines (see Fig. 7c).

QMAH and QCRP tended to be similar in their responses to reductions in return densities (see Fig. 6a and b). There were underestimations of the metrics towards lower-density data; however, the slope and the intercepts of the fitted lines remained close to 1 and 0, respectively. The correlation with the original resolution metrics was still high with R^2 of more than 0.9 at a return density of 1/16. At the density of 1/5 returns per m^2, the slope and R^2 were very close to 1. Further sharp declines in accuracy occurred at the return density of 1/100. However, QMAH metrics were unable to detect most of the low vegetation areas at a return density lower than 1/16.

3.4. Return density effects on model-based estimates of mean AGB

To assess the effect of decreasing the lidar return density on the precision of the AGB estimates at landscape scale, the (model-based) mean ABG estimate was calculated over the study area ($\frac{1}{N}\sum_{i=1}^{N}\hat{\mu}_i$) and the (approximate) variance of this estimator ($\frac{1}{n_{grid}{}^2}\sum_{i=1}^{n_{grid}}\sum_{j=1}^{n_{grid}}\mathbf{Z}_{\mathbf{i}}^{'}\mathbf{V}_{\hat{\beta}}\mathbf{Z}_{\mathbf{j}}$) for the original density (2.8 returns per m^2) and densities corresponding to four thinning levels (1/4, 1/16, 1/49, and 1/100 returns per m^2) (see Table 5). The standard deviation was reported; thus, the units were the same as the mean estimate. In this case, the variance was calculated using a gridded sample with a spacing of $n_p = 50$ (30 m × 50 = 1500 m), resulting in $n_{grid} = 525$. The mean AGB was calculated using all ($N = 1{,}330{,}748$) pixels for each density level.

Table 6
Mean AGB estimates, SEs and REs of mean AGB estimates for different simulated lidar densities. RE is the relative difference of the mean AGB from the mean AGB of the highest density model.

Lidar density	Mean AGB estimate (Mg ha^{-1})	SE in Mg ha^{-1} [% SE]	RE (%)
2.8	202.41	6.31 [3.1%]	–
1/4	188.85	17.63 [9.3%]	−6.7
1/16	198.03	22.70 [11.5%]	−2.2
1/49	190.04	25.94 [13.7%]	−6.1
1/100	198.62	40.40 [20.3%]	−1.9

The model-based estimated mean AGB using the highest density dataset was 202.41 Mg ha^{-1} with a relative standard error (SE) of only 3.1% (see Table 6). The relative errors (RE) of the estimates from reduced density datasets ranged from −1.9% to −6.7%. The precision of the model-based estimate of mean AGB decreased as the return density decreased. However, at the study site, the relatively precise estimates of the mean AGB (13.7% relative SE) were still obtained with a fairly low-density of 1/49 returns per m^2.

4. Discussions

This study showed that models with return proportion metrics appeared to better predict AGB in PSF than models with height-related metrics. Our analysis suggested that the cumulative value of return proportions better represents the accumulation of biomass

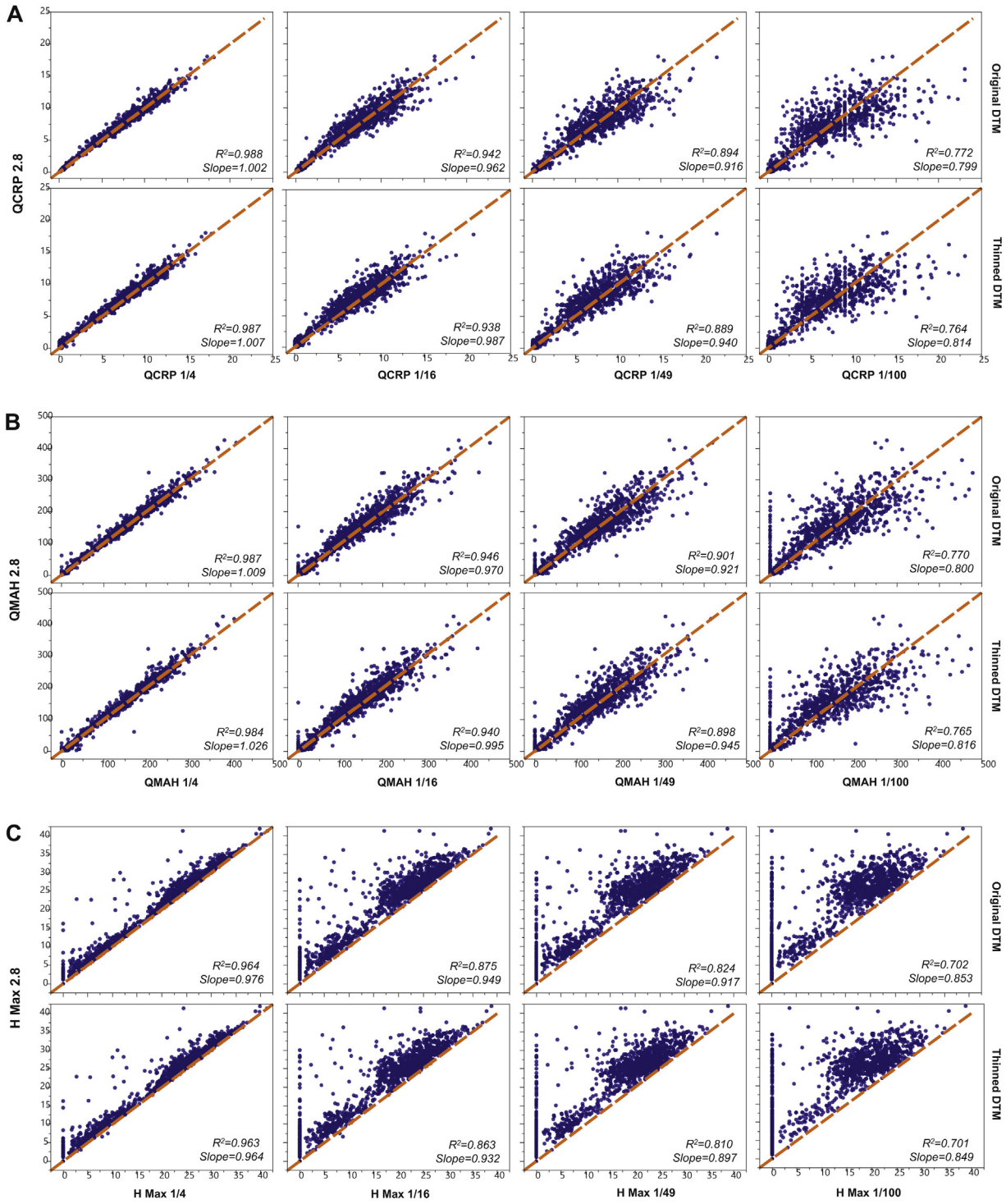

Fig. 7. Comparison of the highest density and the reduced density metrics: (a) QCRP, (b) QMAH and (c) H Max.

along the canopy height bins than the height-related statistics. The models with return proportion metrics not only provided the highest R^2 and the lowest RMSE, but also had normal distribution of errors. Ioki et al. (2014) used return proportions below a height of 12 m as a predictor variable and found that it explained more than 70% of AGB variation in tropical Bornean forests. (Sheridan et al., 2014) also analysed the return proportions above certain heights to estimate AGB in conifer-dominated forests of Oregon. Both studies concluded that the best model was not the model with the return proportion variable. Those studies used return proportion or return number at certain height bins as a single variable, rather than the cumulative return proportion (CRP) as used in this study.

Several authors have suggested using linear models by using a square root transformation for the dependent variables and then back transforming the prediction using correction factors (d'Oliveira et al., 2012; Sheridan et al., 2014). However, this study found the use of quadratic (squared) terms for independent variables; that is, QCRP was more parsimonious than transforming the dependent variables, as it did not require a back transformation. In this study, the models with square root transformed dependent

variables had higher R^2 values. However, the back-transformed models were slightly worse than the models with squared independent variables.

Similar to previous research (Gobakken and Næsset, 2008), this study showed that reducing return density had the greatest effect on the H max metric and led to biased estimates of the forest metrics. As the return density was reduced, the probability of the lidar pulse hitting the highest point of the vegetation canopy decreased. Thus, it appeared that H max is sensitive to decreases in low return density and should not be used as an independent variable for developing models for forest metrics, particularly, in relation to low-density lidar datasets.

This study suggested that using a thinned DTM provided similar accuracies to those obtained using the original DTM to normalise the lidar point elevations in PSF. However, other studies conducted on relatively complex terrain (Leitold et al., 2015; Watt et al., 2014) showed that DTM from lower-density datasets had lower precision, as the percentage of classified ground points increased as return density fell. The study area was very flat, with slope less than 0.1%; thus, a lack of complex topography may explain this contradiction. However, Hansen (Hansen et al., 2015) found that low return density of up to 1/4 returns per m^2 had little effect on DTM in tropical mountainous regions and further suggested that the accuracy in ground point classification was crucial.

Reducing return density to approximately 1/4–1/9 returns per m^2 yielded model accuracies comparable to those obtained with higher return densities. A relatively precise estimate (with relative SE less than 10%) of the mean AGB at landscape scale were still obtained with a fairly low-density of 1/4 returns per m^2 using model-based statistical inference. Thus, it appears that potentially acceptable biomass and carbon estimates can be obtained in very flat regions using low-density ALS. Further, by using very low-density ALS data (1/49 returns per m^2), the bias of the mean AGB estimates remained less than 10% and had a SE of less than 14%. In relation to reducing return density in PSF, the results were much more promising than those of previous studies in areas with relatively complex topography (Jakubowski et al., 2013; Leitold et al., 2015) and their accuracy was similar to that of a study in relatively flat areas in temperate forests (Gobakken and Næsset, 2008). However, it should be noted that these conclusions should not be extended to more mountainous areas, as the deleterious effects of lower return density on the quality of biomass estimates may be much more evident (see the discussion above). These findings suggest that high-density ALS is not required for forests and AGB monitoring in flat tropical PSF. Thus, the costs of remote sensing assisted forest monitoring could be reduced if less expensive, lower-density ALS data were used.

For area-based forest monitoring, (e.g for AGB, BA, timber volume) such approach using low density lidar might be appropriate with consideration of the terrain factor. In flat terrain, model-based inference using return density of 0.02–0.05 would still yield 85% accuracy, as suggested from this study and Strunk et al. (2012). In a relatively steep and complex terrain, a 0.25 return density still provides a similar level of accuracy (for forest metric estimates) as high density lidar (Gobakken and Næsset, 2008; Ruiz et al., 2014). However in very steep terrain and mountainous region, high density lidar seems to be required to avoid error in DTM (Leitold et al., 2015).

5. Conclusions

This study demonstrated that low-density ALS is a feasible option for assessing AGB in vast areas of flat, lowland PSF. Notably, this study showed that return proportion-related variables (i.e., CRP, QCRP and CStr) were able to estimate AGB and BA better than height-related variables. Those variables represent better accumulation of AGB over tree heights. This study provided strong evidence that the accuracy of the models generated using data with lower return densities of 1/9 returns per m^2 still yielded strong agreement with models generated using the original, higher-density data. Using variance estimator approach, the bias and standard error of the mean AGB at the landscape level, estimate using 1/49 returns per m^2 data were less than 10% and 15%, respectively. This study also showed that a high-resolution DTM had little effect on the accuracy of the calculated lidar metrics for areas with terrain similar to that examined in this study. Consequently, the acquisition and processing costs could be reduced if large areas of tropical PSF were monitored with ALS while maintaining relatively good accuracy.

Acknowledgements

This study was funded by the United States Government's SilvaCarbon programme. The authors are grateful to the KFCP project, a bilateral project between Indonesia and Australia governments and the Ministry of Forestry of Indonesia for providing the lidar and plot measurement datasets and to Pavla Graham and Laura Graham for their guidance in accessing plot measurement data. We would also like to acknowledge the support of Professor Monika Moskal and the team from Remote Sensing and Geospatial Analysis Laboratory of the University of Washington, United States who provided resources and suggestions during data processing. We thank Julie Watson for their critical reading of the previous manuscript, Elite Editing for proof reading of the draft manuscript and the two anonymous reviewers for their insightful comments and suggestions to improve the manuscript. We also thank Clive Hilliker for the support in graphic editing. Solichin Manuri gratefully acknowledges the support of Australia Award Scholarship from 2013 to 2017.

Appendix A. Supplementary data

Supplementary data associated with this article can be found, in the online version, at http://dx.doi.org/10.1016/j.jag.2016.11.002.

References

Andersen, H.-E., Reutebuch, S.E., McGaughey, R.J., 2006. A rigorous assessment of tree height measurements obtained using airborne lidar and conventional field methods. Can. J. Remote Sens. 32, 355–366.

Andersen, H.-E., Reutebuch, S.E., McGaughey, R.J., d'Oliveira, M.V., Keller, M., 2014. Monitoring selective logging in western Amazonia with repeat lidar flights. Remote Sens. Environ. 151, 157–165.

Anderson, J., 1963. The flora of the peat swamp forests of Sarawak and Brunei including a catalogue of all recorded species of flowering plants, ferns and fern allies. Gardens Bull. Singapore 20, 131–228.

Asner, G.P., Mascaro, J., 2014. Mapping tropical forest carbon: calibrating plot estimates to a simple LiDAR metric. Remote Sens. Environ. 140, 614–624.

Ballhorn, U., Navratil, P., Jubanski, J., Siegert, F., 2014. Lidar survey of the Kalimantan Forests and Climate Partnership (KFCP) project site and EMRP area in Central Kalimantan, Indonesia. Technical Working Paper. Kalimantan Forests and Climate Partnership.

d'Oliveira, M.V.N., Reutebuch, S.E., McGaughey, R.J., Andersen, H.-E., 2012. Estimating forest biomass and identifying low-intensity logging areas using airborne scanning lidar in Antimary State Forest, Acre State, Western Brazilian Amazon. Remote Sens. Environ. 124, 479–491.

Drake, J.B., Knox, R.G., Dubayah, R.O., Clark, D.B., Condit, R., Blair, J.B., Hofton, M., 2003. Above-ground biomass estimation in closed canopy neotropical forests using lidar remote sensing: factors affecting the generality of relationships. Global Ecol. Biogeogr. 12, 147–159.

Englhart, S., Keuck, V., Siegert, F., 2011. Aboveground biomass retrieval in tropical forests—the potential of combined X- and L-band SAR data use. Remote Sens. Environ. 115, 1260–1271.

Englhart, S., Jubanski, J., Siegert, F., 2013. Quantifying dynamics in tropical peat swamp forest biomass with multi- temporal LiDAR datasets. Remote Sens. 5, 2368–2388.

Gobakken, T., Næsset, E., 2008. Assessing effects of laser point density, ground sampling intensity, and field sample plot size on biophysical stand properties derived from airborne laser scanner data. Can. J. For. Res. 38, 1095–1109.

Goodwin, N.R., Coops, N.C., Culvenor, D.S., 2006. Assessment of forest structure with airborne LiDAR and the effects of platform altitude. Remote Sens. Environ. 103, 140–152.
Graham, L.L.B., Susanto, T.W., Xaveius, F., Eser, E., Didie, Salahuddin, Mahyudi, A., Applegate, G., 2014. KFCP Vegetation Monitoring: Rates of change for forest characteristics and the influence of environmental conditios n the KFCP study area. Kalimantan Forests and Climate Partnership Scientific Report.
Hansen, E.H., Gobakken, T., Næsset, E., 2015. Effects of pulse density on digital terrain models and canopy metrics using airborne laser scanning in a tropical rainforest. Remote Sens. 7, 8453–8468.
Hergoualc'h, K., Verchot, L., 2014. Greenhouse gas emission factors for land use and land-use change in Southeast Asian peatlands. Mitig. Adapt. Strat. Gl. 19, 789–807.
Hirata, Y., Tabuchi, R., Patanaponpaiboon, P., Poungparn, S., Yoneda, R., Fujioka, Y., 2014. Estimation of aboveground biomass in mangrove forests using high-resolution satellite data. J. For. Res. 19, 34–41.
Hooijer, A., Silvius, M., Wosten, H., Page, S., 2006. PEAT-CO2, Assessment of CO2 emissions from drained peatlands in SE Asia. Delft Hydraulics report Q3943/2006.
Houghton, R., House, J., Pongratz, J., van der Werf, G., DeFries, R., Hansen, M., Quéré, C.L., Ramankutty, N., 2012. Carbon emissions from land use and land-cover change. Biogeosciences 9, 5125–5142.
Hummel, S., Hudak, A., Uebler, E., Falkowski, M., Megown, K., 2011. A comparison of accuracy and cost of LiDAR versus stand exam data for landscape management on the Malheur National Forest. J. For. 109, 267–273.
Ichsan, N., Vernimmen, R., Hooijer, A., Applegate, G., 2013. KFCP Hydrology and Peat Monitoring Methodology. Technical Working Paper. Kalimantan Forests and Climate Partnership.
Ioki, K., Tsuyuki, S., Hirata, Y., Phua, M.H., Wong, W.V.C., Ling, Z.Y., Saito, H., Takao, G., 2014. Estimating above-ground biomass of tropical rainforest of different degradation levels in Northern Borneo using airborne LiDAR. For. Ecol. Manage. 328, 335–341.
Jakubowski, M.K., Guo, Q., Kelly, M., 2013. Tradeoffs between lidar pulse density and forest measurement accuracy. Remote Sens. Environ. 130, 245–253.
Jubanski, J., Ballhorn, U., Kronseder, K., Franke, J., Siegert, F., 2012. Detection of large above ground biomass variability in lowland forest ecosystems by airborne LiDAR. Biogeosci. Discuss. 9, 11815–11842.
Kohavi, R., 1995. A study of cross-validation and bootstrap for accuracy estimation and model selection. IJCAI, 1137–1145.
Lefsky, M.A., Hudak, A.T., Cohen, W.B., Acker, S., 2005. Geographic variability in lidar predictions of forest stand structure in the Pacific Northwest. Remote Sens. Environ. 95, 532–548.
Leitold, V., Keller, M., Morton, D.C., Cook, B.D., Shimabukuro, Y.E., 2015. Airborne lidar-based estimates of tropical forest structure in complex terrain: opportunities and trade-offs for REDD+. Carbon Balance and Manage. 10, 1.
Magnusson, M., Johan, E.S.F., Holmgren, J., 2007. Effects on estimation accuracy of forest variables using different pulse density of laser data. For. Sci. 53, 619.
Manuri, S., Brack, C., Nugroho, N.P., Hergoualc'h, K., Novita, N., Dotzauer, H., Verchot, L., Putra, C.A.S., Widyasari, E., 2014. Tree biomass equations for tropical peat swamp forest ecosystems in Indonesia. For. Ecol. Manage. 334, 241–253.
Manuri, S., Joseph, S., Martius, C., Brack, C., 2015. Uncertainties of above ground biomass estimates in tropical peat swamp forest. In: Paper prepared for International Conference of Indonesia Forestry Researchers III-2015 (3rd INAFOR 2015), 21–22 October 2015. Forestry Research and Development Agency, INAFOR, Bogor, Indonesia.
McGaughey, R., 2014. FUSION/LDV: Software for LIDAR Data Analysis and Visualization USDA Forest Service. Pacific Northwest Research Station.
McRoberts, R.E., 2010. Probability-and model-based approaches to inference for proportion forest using satellite imagery as ancillary data. Remote Sens. Environ. 114, 1017–1025.
McRoberts, R.E., Naesset, E., Gobakken, T., 2013. Accuracy and precision for remote sensing applications of nonlinear model-based inference. IEEE J. Sel. Topics Appl. Earth Observ. in Remote Sens. 6, 27–34.
Miettinen, J., Shi, C., Liew, S.C., 2012. Two decades of destruction in Southeast Asia's peat swamp forests. Front. Ecol. Environ. 10, 124–128.
MoEF, 2015. National Forest Reference Emission Level for Deforestation and Forest Degradation: In the Context of Decision 1/CP.16 para 70 UNFCCC (Encourages Developing Country Parties to Contribute to Mitigation Actions in the Forest Sector) Directorate General of Climate Change. The Ministry of Environment and Forestry, Indonesia.
Morley, R.J., 1981. Development and vegetation dynamics of a lowland ombrogenous peat swamp in Kalimantan Tengah, Indonesia. J. Biogeogr., 383–404.
Murdiyarso, D., Hergoualc'h, K., Verchot, L., 2010. Opportunities for reducing greenhouse gas emissions in tropical peatlands. Proc. Natl. Acad. Sci. 107, 19655–19660.
Næsset, E., 2004. Effects of different flying altitudes on biophysical stand properties estimated from canopy height and density measured with a small-footprint airborne scanning laser. Remote Sens. Environ. 91, 243–255.
Page, S.E., Rieley, J.O., Shotyk, Ø.W., Weiss, D., 1999. Interdependence of peat and vegetation in a tropical peat swamp forest. Philos. Trans. R. Soc. Lonn. Ser. B: Biol. Sci. 354, 1885–1897.
Page, S.E., Siegert, F., Rieley, J.O., Boehm, H.-D.V., Jaya, A., Limin, S., 2002. The amount of carbon released from peat and forest fires in Indonesia during 1997. Nature 420, 61–65.
Page, S., Wűst, R., Weiss, D., Rieley, J., Shotyk, W., Limin, S.H., 2004. A record of Late Pleistocene and Holocene carbon accumulation and climate change from an equatorial peat bog (Kalimantan, Indonesia): implications for past, present and future carbon dynamics. J. Quat. Sci. 19, 625–635.
Page, S.E., Rieley, J.O., Banks, C.J., 2011. Global and regional importance of the tropical peatland carbon pool. Global Change Biol. 17, 798–818.
T.R-Development-Core, 2013. R: A Language and Environment for Statistical Computing. R Foundation for Statistical Computing, Vienna, Austria.
Rieley, J., Ahmad-Shah, A., 1996. The Vegetation of Tropical Peat Swamp Forests. Tropical Lowland Peatlands of Southeast Asia, pp. 55–74.
Roxburgh, S., Paul, K., Clifford, D., England, J., Raison, R., 2015. Guidelines for constructing allometric models for the prediction of woody biomass: how many individuals to harvest? Ecosphere 6, 1–27.
Ruiz, L.A., Hermosilla, T., Mauro, F., Godino, M., 2014. Analysis of the influence of plot size and LiDAR density on forest structure attribute estimates. Forests 5, 936–951.
SAS, I.I., 2015. Using JMP 12. SAS Institute Inc., Cary, NC.
Schlund, M., von Poncet, F., Kuntz, S., Schmullius, C., Hoekman, D.H., 2015. TanDEM-X data for aboveground biomass retrieval in a tropical peat swamp forest. Remote Sens. Environ. 158, 255–266.
Sheridan, R.D., Popescu, S.C., Gatziolis, D., Morgan, C.L., Ku, N.-W., 2014. Modeling forest aboveground biomass and volume using airborne LiDAR metrics and forest inventory and analysis data in the Pacific Northwest. Remote Sens. 7, 229–255.
Siegert, F., Ruecker, G., Hinrichs, A., Hoffmann, A.A., 2001. Increased damage from fires in logged forests during droughts caused by El Niño. Nature 414, 437–440.
Sileshi, G.W., 2014. A critical review of forest biomass estimation models, common mistakes and corrective measures. For. Ecol. Manage. 329, 237–254.
Singh, K.K., Chen, G., McCarter, J.B., Meentemeyer, R.K., 2015. Effects of LiDAR point density and landscape context on estimates of urban forest biomass. ISPRS J. Photogramm. Remote Sens. 101, 310–322.
Strunk, J., Temesgen, H., Andersen, H.-E., Flewelling, J.P., Madsen, L., 2012. Effects of lidar pulse density and sample size on a model-assisted approach to estimate forest inventory variables. Can. J. Remote Sens. 38, 644–654.
Watt, M.S., Meredith, A., Watt, P., Gunn, A., 2014. The influence of LiDAR pulse density on the precision of inventory metrics in young unthinned Douglas-fir stands during initial and subsequent LiDAR acquisitions. N. Z. J. For. Sci. 44, 18.
Zanne, A., Lopez-Gonzalez, G., Coomes, D., Ilic, J., Jansen, S., Lewis, S., Miller, R., Swenson, N., Wiemann, M., Chave, J., 2009. Global wood density database. Dryad 235, Identifier: http://hdl.handle.net/10255/dryad (accessed 1 February 2014).